Charge within Nt17 peptides modulates huntingtin aggregation and initial lipid binding events

Alyssa R. Stonebraker[1], Rachel Hankin[1], Kathryn L. Kapp[1], Peng Li[1], Stephen J. Valentine[1], and Justin Legleiter[1,2,3,]*

[1]The C. Eugene Bennett Department of Chemistry, West Virginia University, 217 Clark Hall, Morgantown, West Virginia 26506, USA
[2]Rockefeller Neurosciences Institutes, West Virginia University, 1 Medical Center Dr., P.O. Box 9303, Morgantown, West Virginia 26505, USA
[3]Department of Neuroscience, West Virginia University, 1 Medical Center Dr., P.O. Box 9303, Morgantown, West Virginia 26505, USA

*To whom correspondence should be addressed: Email: Justin.legleiter@mail.wvu.edu

HIGHLIGHTS

- Htt-exon1(46Q) fibril formation is inhibited by free Nt17 peptides.
- Incorporation of free Nt17 peptides alters oligomer morphology.
- Modifications within Nt17 alter peptide/lipid complexation.
- Nt17 peptide-containing oligomers demonstrate altered lipid interactions.

KEYWORDS

Huntington's disease, amyloid, post-translational modification, atomic force microscopy, mass spectrometry

ABSTRACT

Toxic aggregation of pathogenic huntingtin protein (htt) is implicated in Huntington's disease and influenced by various factors, including the first seventeen amino acids at the N-terminus (Nt17) and the presence of lipid membranes. Nt17 has a propensity to form an amphipathic α-helix in the presence of binding partners, which promotes α-helix rich oligomer formation and facilitates htt/lipid interactions. Within Nt17 are multiple sites that are subject to post-translational modification, including acetylation and phosphorylation. Acetylation can occur at lysine 6, 9, and/or 15 while phosphorylation can occur at threonine 3, serine 13, and/or serine 16. Such modifications impact aggregation and lipid binding through the alteration of various intra- and intermolecular interactions. When incubated with htt-exon1(46Q), free Nt17 peptides containing point mutations mimicking acetylation or phosphorylation reduced fibril formation and altered oligomer morphologies. Upon exposure to lipid vesicles, changes to peptide/lipid complexation were observed and peptide-containing oligomers demonstrated reduced lipid interactions.

INTRODUCTION

Huntington's disease (HD) is a fatal neurodegenerative disease resulting from an expansion in the poly-glutamine (polyQ) domain within the huntingtin (htt) protein.[1] The expansion of the polyQ domain beyond a threshold of approximately 35 repeats[2, 3] causes htt to aggregate into amyloid-like fibrils.[4-6] The aggregation pathway is very complex and involves various aggregate species, including oligomers and amorphous aggregates.[7] Sequences directly adjacent to the polyQ domain of the protein, including the first 17 amino acids at the N-terminus (Nt17), heavily influence htt interactions with respect to both

aggregation[8-10] and lipid binding. [11-14] Htt is an intrinsically disordered protein,[15, 16] but the Nt17 domain has a propensity to form an amphipathic α-helix that facilitates early interactions of htt through intermolecular association, promoting the formation of α-helix rich oligomers. [17-21] Within these oligomers, polyQ domains are brought into close proximity, promoting fibril nucleation.[20, 22]

The Nt17 domain also facilitates lipid interactions and subsequent damage through its ability to form an amphipathic α-helix.[13, 23] Many of the normal functions attributed to htt, including vesicle transport and synaptic transmission,[24, 25] require interactions with a variety of lipid membrane systems. Specifically, htt associates closely with the endoplasmic reticulum (ER),[26-28] mitochondrial,[29-33] nuclear,[27, 28, 34] and plasma[35] membranes. Mutant htt aggregation damages organelle membranes. Inclusions interact with the ER, resulting in membrane deformation, impaired organization, and altered dynamics of the membrane.[36] Damaged and fragmented mitochondria accumulate at the periphery of htt inclusions and have increased respiration rates.[37] Interactions of htt at the nuclear envelope exacerbate age-related degeneration of the membrane and impairs nucleocytoplasmic transport.[38]

Both aggregation and interactions between Nt17 and lipids are modulated by a variety of factors, including lipid composition. Compared to aggregation in bulk solution, total brain lipid extract (TBLE)[39] and cellular lipid extracts[40] reduce htt fibrillization. Some pure lipid systems, such as palmitoyl-2-oleoyl-glycero-3-phosphocholine (POPC)[39, 41] and a mixture also containing 1-palmitoyl-2-oleoyl-sn-glycero-3-phospho-L-serine (POPS)[42] enhance fibril formation, with the POPC/POPS system promoting a unique aggregation pathway facilitated by Nt17 versus aggregation observed in the absence of lipid.[42] Conversely, 1,2,-dioleoyl-sn-

glycero-3-phosphocholine (DOPC) inhibits fibril formation.[41] Lipid physiochemical properties play a large role in htt/lipid interactions, with htt demonstrating preferential interactions with anionic phospholipids compared to zwitterionic lipids.[14, 43] Additionally, while changes to lipid tail groups did not display a direct correlation between aggregation and htt/lipid complexation, it was revealed that membrane defect sizes in conjunction with Nt17 orientation and hydrophobic residue sizes are critical to lipid interactions.[41] Changes to lipid composition by additional lipid components, including ganglioside (GM1) and sphingomyelin (SM) content, further modulate htt/lipid with the addition of either GM1 or SM to TBLE, reducing the insertion of htt into the membrane and promoting unique aggregate morphologies.[44]

A second modulating factor of htt interactions are several sites within Nt17 that are subject to post-translational modifications (PTMs). Such modifications include phosphorylation, [45-48] acetylation, [46, 49] ubiquitination,[50] and SUMOylation.[51] PTMs at these sites alter both the aggregation propensity[45, 46, 48, 49, 52] and lipid interactions[49, 52, 53] of htt. Specifically, phosphorylation within Nt17 reduces aggregate accumulation,[54] while lysine acetylation decreased the formation of large, globular oligomers and reduced membrane damage by altering Nt17/lipid association.[49] Peptides with other mutations have also been used as mutant htt inhibitors; the incubation of htt with analogs of human Nt17 and sequence variants from evolutionarily distant organisms inhibited aggregation,[55] while other Nt17 derived peptides, especially those containing D-amino acids and sequences where cell penetrating sequences were attached, inhibited nucleation and subsequent aggregation.[22]

Aggregation is dependent on a variety of factors, including the presence of lipids and their composition in addition to post-translational modifications within the Nt17 domain.

Considering the close association of htt with a variety of membrane systems and subsequent damage observed in HD, understanding htt-lipid interactions and how such interactions can be modulated is crucial to gaining a better understanding of the toxic mechanism and pathogenesis. Using the ability of truncated Nt17-derived peptides to inhibit fibril formation,[22] our aim was to identify how the incorporation of modified Nt17-derived peptides, with altered net charges, into htt oligomers structures modulates aggregation, lipid binding, and htt/lipid complexation.

METHODS

Preparation of synthetic peptides. Synthetic Nt17 peptides were obtained via custom synthesis by GenScript. These peptides and their sequences are indicated in Figure 1a. Based on analysis provided by GenScript, peptide purities ranged from 95-98.6%. Peptides were solubilized in dimethyl sulfoxide (DMSO) to a stock concentration of 2,000 µM. Solubilized peptide was stored at -20 ^{o}C until needed. On the day of the experiment, solubilized peptide was thawed and diluted to the desired final concentration such that the concentration of DMSO was less than 1% in the final solution.

GST-htt-exon1 fusion protein purification. Disease length (46Q) glutathione S-transferase (GST)-htt-exon1 fusion protein (Figure 1b) was purified as previously described using the pGEX-5X-1 vector.[56, 57] In short, GST-htt fusion proteins were expressed by induction in *Escherichia coli* with isopropyl-thio-galactopyranoside (IPTG) at 30 °C for 4 h. Cells were lysed using lysozyme (0.5 mg/mL) and sonication with a sonic dismembrator (FisherSci). Liquid chromatography (BioRad LPLC) with a GST affinity column was then used to purify the fusion proteins and the concentration was determined with Coomassie Bradford reagent. High speed

centrifugation at 20,000 g for 45 min at 4 °C removed any preexisting aggregates from fusion protein solutions. Incubation of fusion proteins with Factor Xa (Promega, Madison, WI) cleaved the GST tag and initiated aggregation for experiments.

Lipid vesicle preparation. Lyophilized lipids of POPC, POPS, and TBLE were dissolved in chloroform and aliquoted into Eppendorf tubes. Aliquots were allowed to dry overnight, and the dry films were stored at -20 °C until needed. POPC and POPS aliquots were redissolved in chloroform and mixed to obtain 75/25% w/w PC/PS samples, which were dried overnight and stored at -20 °C until needed. For experiments, the dried films were rehydrated in tris buffer (150 mM NaCl, Tris-HCl, pH 7.4) for 1 h at 30 °C. Rehydrated lipids were subjected to 10 freeze-thaw cycles using liquid nitrogen. Lipid solutions were then bath sonicated for 1 h and stored at 4 °C.

Thioflavin T (ThT) aggregation assays. ThT assays were used to monitor fibril formation of htt-exon1(46A) incubated with and without various Nt17 peptides. For all conditions htt-exon1(46Q) (10 µM) was incubated with ThT (125 µM) in black Costar 96-well plates with flat, clear bottoms. For conditions with Nt17 peptides, 10 µM of each peptide was added, resulting in an $Nt17Q_{35}P_{10}$:peptide ratio of 1:1. Assays were performed using a SpectraMax M2 microplate reader where ThT fluorescence was measured at 37 °C using excitation and emission wavelengths of 440 nm and 480 nm, respectively. Emission data was collected every 10 min over 18 h. A blank sample containing no peptide was used to collect background fluorescence and correct for background. Samples were run in triplicate and averaged.

Polydiacetylene (PDA) lipid binding assays. Htt-exon1(46Q) interactions with lipids were measured using a PDA lipid binding assay using previously reported protocol.[58] Briefly,

diacetylene monomers of 10,12-tricosadiynoic acid and the lipid system of choice were mixed at a 2:3 molar ratio in 4:1 chloroform/ethanol solution. The solution was evaporated off to yield dry lipid films that were reconstituted in 70 °C tris buffer. Lipid solutions were sonicated (amplitude 50) for 10 min using a dismembrator (FisherSci) and stored overnight at 4 °C to allow for self-assembly of vesicles. For experiments, lipid mixtures were irradiated at 254 nm for 10 min with constant stirring to polymerize the 10,12-tricosadiynoic acid, resulting in a dark blue solution which undergoes a colorimetric shift to red with increased fluorescence when exposed to mechanical stress. Experimental conditions were performed in triplicate in black Costar 96-well plates with flat, clear bottoms. Assays were performed using a SpectraMax M2 microplate reader where fluorescence was measured at 25 ^{o}C every 10 min over 18 h using excitation and emission wavelengths of 489 nm and 570 nm, respectively. The positive control included saturated NaOH (pH 12) while the negative control consisted of PDA/lipid vesicles and tris buffer. Mutant Nt17 peptides were incubated with htt-exon1 in a 1:1 ratio for 3 h to obtain peptide-containing oligomers. Polymerized vesicles were exposed to htt-exon1(46Q) oligomers at a final concentration of 10 μM. Samples were run in triplicate and averaged.

Atomic force microscopy (AFM). Purified htt-exon1(46Q) (10 μM) was incubated with Nt17 peptides in a 1:1 protein:peptide ratio in the absence of lipids at 37 °C and 1,400 rpm using an orbital mixer. At selected time points, a 2 μL aliquot of each condition was deposited onto freshly cleaved mica and allowed to sit for 1 min. Mica was then washed with 200 μL of ultra-pure water and dried with a gentle stream of air. All images were collected with a Nanoscope V Multi-Mode scanning probe microscope (Veeco, Santa Barbara, CA) equipped with a closed loop vertical engage J-scanner. Silicon-oxide cantilevers with 300 kHz resonance frequency and

40 N/m nominal spring constant were used. Scan rates were set between 1 and 2 Hz with cantilever drive frequencies at 10% of resonance.[59] All images were collected with 512 x 512 pixel resolution. The Matlab image processing toolbox (MathWorks) was used to analyze oligomer morphology as previously described.[60, 61] In short, a height threshold of 0.8 nm was used to create binary maps to locate objects in the AFM images. This threshold value was chosen because the GST-htt-exon1(46Q) system used in this study has residual GST which results in a granular background in the AFM images of RMS ~0.6 nm. The 0.8 nm eliminates including artifacts associated with GST from the analysis. However, this also means that htt aggregates shorter than 0.8 nm will not be detected either. To be included in the analysis, an object must contain at least 10 pixels. Every object identified in the AFM image is assigned a tracking number, and this number is plotted onto the AFM image to assure that all objects are measured (Figure S1). As some large, non-oligomer aggregates are presented in some of the images, additional filters based on morphology can be implemented to remove these from the resulting data set. In this instance, oligomers were defined of having 50 (~4,700 nm^2 of surface area) or fewer pixels associated with them. All morphology data on oligomers is compiled from two independent experiments with at least five images taken at the 3 h time point used for analysis.

Pulled-tip capillary emitter and capillary vibrating sharp-edge spray ionization (cVSSI) device fabrication. Descriptions of cVSSI devices have been provided previously.[62, 63] Briefly, epoxy glue was used to secure a piezoelectric transducer to the end of a glass slide coverslip. A glass capillary emitter (0.5 mm I.D.) was pulled (Sutter Instrument Company, Novato, CA) and cut mechanically to the desired I.D. (70-100 μm) verified under a microscope. The emitter tip was

secured to the glass slide coverslip opposite the piezoelectric transducer with glass glue. Using epoxy glue, a fused silica capillary section (250 µm I.D., 355 µm O.D.) was inserted into the glass emitter and secured at the flat end. PTFE tubing was attached to the fused silica capillary at one end and secured to a syringe at the other to allow for sample infusion. A 5 cm platinum wire inserted into the end of the PTFE tubing nearest to the cVSSI device and secured with epoxy glue served as an electrode for field-enabled experiments.

Capillary vibrating sharp-edge electrospray ionization-mass spectrometry (cVSSI-MS). Mutant Nt17 peptides (10 µM) were incubated with PC/PS (75/25% w/w) lipid vesicles in a 1:10 ratio (peptide:lipid) at 37 ^{o}C for 5 h. Lipid vesicles were formed by rehydrating lipid films in 10 mM ammonium acetate, which were then subjected to 10 freeze-thaw cycles using liquid nitrogen followed by bath sonication for 1 h. Samples were analyzed using cVSSI devices and a Q-Exactive hybrid quadrupole Orbitrap (Thermo Fisher, San Jose, CA) mass spectrometer. Spectra were collected in positive ion mode over a mass-to-charge (m/z) range of 300 to 4,000. Samples were infused at a rate of 10 µL/min with 1.8 kV applied to the Pt wire. The resolving power and AGC target were set to 70,000 and $1x10^{6}$, respectively. The inlet capillary temperature was maintained at 250 °C. Mass spectra were recorded in triplicate for 30 s each. Between spectra collections, the voltage supply to the cVSSI device was turned off, and the sample was allowed to flow without voltage. Turning off the voltage between collections took into account any variability across triplicate spectra, represented as the standard error of the mean (SEM), that may result from changing devices or variations in plume generation and droplet sizes. Data were analyzed using the Xcalibur 2.2 software suite (Thermo Scientific).

RESULTS & DISCUSSION

Incorporation of modified Nt17 peptides inhibits fibril formation and alters oligomer morphologies. Wild type Nt17 peptides inhibit htt aggregation by incorporating into htt oligomers and increasing the spacing between polyQ domains.[22, 55] To determine how the charge-altering point mutations would impact the efficiency of this inhibition of fibril formation, htt-exon1(46Q) (10 μM, Figure 1a) was incubated with Nt17 peptides (Figure 1b) in a 1:1 htt-exon1:Nt17 peptide molar ratio. Nt17 peptides investigated included wild type Nt17, three Nt17-derived peptides with point mutations mimicking acetylation (K6Q, K9Q, or K15Q), and three Nt17-derived peptides with point mutations mimicking phosphorylation (T3D, S13D, or S16D). Fibril formation was monitored as a function of time using ThT, which exhibits enhanced fluorescence when bound to fibril-associated β-sheet structure (Figure 1c). Htt-exon1(46Q) aggregation in the absence of Nt17 peptides was measured for comparison. The ThT signal for each condition was averaged across triplicate runs and normalized to the htt-exon1(46Q) alone control. Additionally, control ThT assays were performed with the truncated Nt17 peptides without the htt-exon1(46Q) (Figure 1d). The Nt17 peptides alone do not induce a ThT signal, as they do not contain a polyQ domain that drives fibril formation.

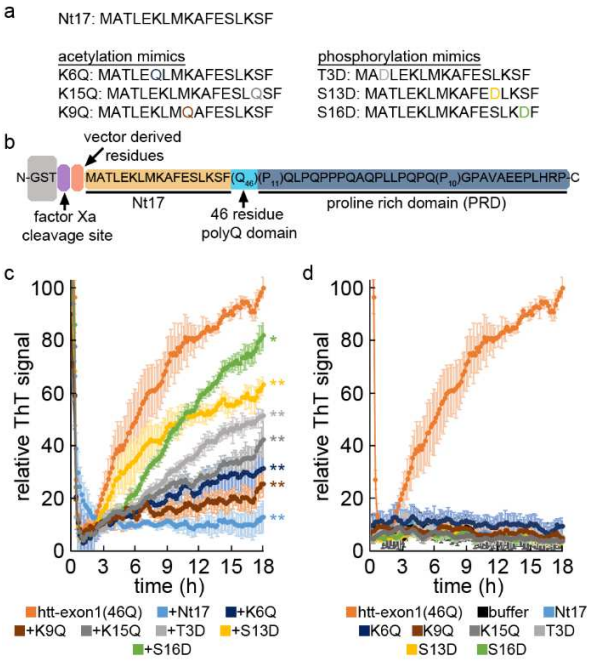

Figure 1: Sequences of the (a) Nt17-derived peptides and (b) GST-htt-exon1(46Q) fusion protein used. For the GST-htt-exon1(46Q) fusion protein, cleavage of GST with factor Xa initiates aggregation. (c) ThT aggregation assay data for htt-exon1 mimic peptide htt-exon1(46Q) incubated alone or with each Nt17 peptide. htt-exon1(46Q) concentration was approximately 10 µM, and incubations with peptide were approximately a 1:1 htt-exon1(46Q):peptide ratio. Conditions were calculated and averaged across all runs, then normalized to the htt-exon1(46Q) control. Error bars represent SEM. Using a Student's t-test, * represents a p-value of <0.05, and ** represents a p-value of <0.01 relative to the htt-exon1(46Q) control. (d) Control ThT assay performed with the Nt17-derived peptides in the absence of htt-exon1(46Q). The control htt-exon1(46Q) ThT response is plotted for reference.

The impact of incubating htt-exon1(46Q) with Nt17 peptides was dependent on the specific Nt17 peptide used, though all peptides significantly reduced fibril formation ($p<0.01$) relative to the Htt-exon1(46Q) control. Wild-type Nt17 peptide, with no mutations, was the most efficient at inhibiting fibril formation. Wild-type Nt17 peptides completely inhibited fibril formation with a 87.1% reduction in signal relative to the htt-exon1(46Q) control. Nt17 peptides containing mutations mimicking acetylation (K6Q, K9Q, or K15Q), which effectively remove a positive charge from within Nt17, were also efficient at inhibiting fibril formation, but less efficient than wild-type Nt17 peptide. Nt17 peptides with K6Q, K9Q, and K15Q reduced

fluorescent signal relative to the htt-exon1(46Q) control by 68.5%, 74.6%, and 57.4%, respectively. Nt17 peptides containing mutations mimicking phosphorylation (T3D, S13D, or S16D), which add a negative charge to Nt17, were the least efficient at inhibiting fibril formation. Relative to the htt-exon1(46Q) control, Nt17 peptides containing T3D, S13D, or S16D resulted in a 48.6%, 36.8%, and 18.0% reduction in signal, respectively.

To further investigate the effect of Nt17 peptide incorporation into htt aggregation, the morphologies of htt-exon1(46Q) aggregates formed in the absence and presence of the different Nt17 peptides was evaluated using AFM (Figures 2). Freshly prepared htt-exon1(46Q) (10 μM) was incubated in the presence and absence of Nt17 peptides in a 1:1 protein:peptide molar ratio and sampled after 3 and 8 h (Figure 2a-b). At 3 h, the dominant aggregate type observed for all conditions was oligomers. The number of fibrils per unit area observed on the mica surface was not statistically different across conditions (Figure 2c). While oligomers were still present for all conditions after 8 h of incubation, fibrils were also present in each condition; however, the fibril density appeared to be lower for incubations of htt-exon1(46Q) with Nt17 peptides. To quantify this, the percent surface area occupied by fibrils was determined (Figure 2d). The surface area coverage was indeed smaller for all incubations of htt-exon1(46Q) with a Nt17 peptide; however, the decrease with S13D and S16D did not reach significance. As it is established that Nt17 peptides incorporate into htt oligomers,[22] the morphologies of the resulting oligomers for all incubations at 3h was further evaluated using automated Matlab scripts that measure morphological features of individually identified oligomers.[61]

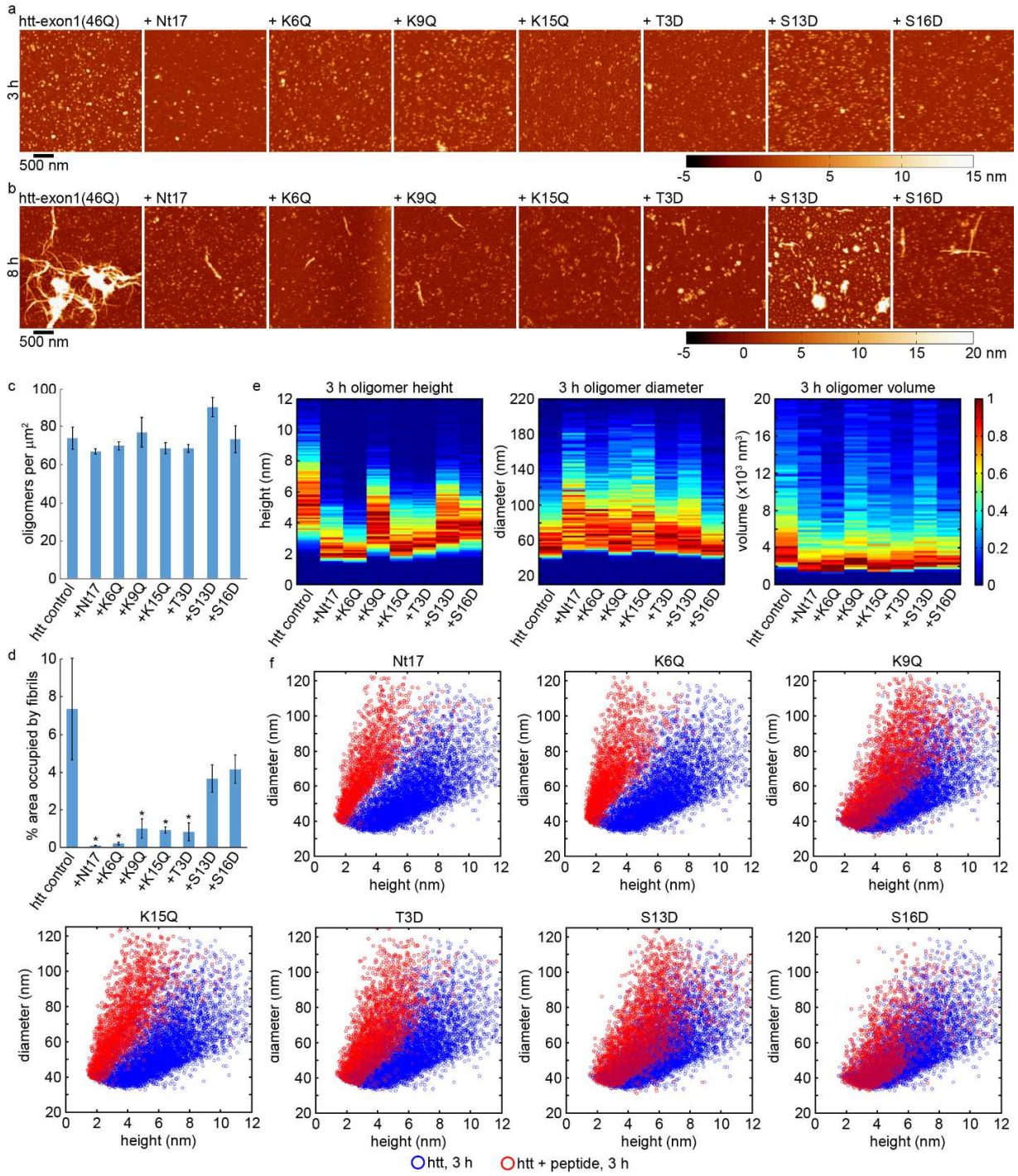

Figure 2: AFM analysis of observed htt-exon1(46Q) aggregates in the absence and presence of each Nt17 peptide. Representative AFM images of 10 µM htt-exon1(46Q) incubated alone or with each Nt17 peptide for (a) 3 h or (b) 8 h. The protein:peptide ratio was 1:1. The colormap and scale bar are applicable to all images. (c) The number of oligomers per µm^2 after 3 h of incubation. The error bars represent SEM (n=5). (d) The percent surface area covered by fibrils after 8 h of incubation. The error bars represent SEM (n=5), and * represents $p < 0.05$ based on a Student's T-test. (e) Histograms of oligomer heights, diameters, and volumes for each

condition. (f) Correlation plots of diameters and heights of each oligomer at 3 h for htt-exon1(46Q) versus htt-exon1(46Q) with each Nt17 peptide.

Oligomer morphology was evaluated by comparing diameters, heights, and volumes of Nt17 peptide-containing oligomers to the pure htt-exon1(46Q) oligomers at 3 h (Figure 2e). Overall, peptide-containing oligomers shifted to smaller heights, slightly larger diameters, and smaller volumes. The pure htt-exon1(46Q) oligomers had a mode height of approximately 5 nm, diameter of 50 nm, and volume of 3.0×10^3 nm^3, while oligomers with incorporation of various Nt17 peptides ranged from 2-4 nm in height, 50-60 nm in diameter, and 2.0×10^3 nm^3 to 3.0×10^3 nm^3 in volume. Based on volume measurements, peptide-containing htt-exon1(46Q) oligomers were smaller. In addition, peptide-containing oligomers were typically shorter (height) but were more spread out (diameters). This could be due to several reasons. The oligomers may just have a different shape associated with incorporation of the truncated peptides, they could have altered surface interactions due to the mutations altering the overall charge of the oligomers, or peptide-containing oligomers could be more easily compressed, e.g., less rigid, in comparison to pure htt-exon1(46Q) oligomers. The potential smaller overall size and reduced aggregate rigidity could be due to the reduction in polyQ and proline-rich domains contained in full-length htt-exon1, as peptide containing oligomers flatten out onto the mica surface. That is, the absence of these domains associated on the peptides could make the oligomers less dense. Looking more closely at oligomer diameter versus height of peptide-containing oligomers compared to pure htt-exon1(46Q) oligomers at 3 h, trends suggesting different peptide incorporation efficiencies emerge (Figure 2f). The most pronounced shift occurred with wild-type Nt17 peptide-containing oligomers, as the peptide-containing

oligomers show virtually no overlap with the pure htt-exon1(46Q) containing oligomers. An intermediate shift occurred with oligomers containing Nt17 peptides with mutations mimicking acetylation (K6Q, K9Q, and K15Q), where slightly more overlap with the pure htt-exon1(46Q) oligomers overall. The smallest shifts occurred with oligomers containing Nt17 peptides with mutations mimicking phosphorylation (T3D, S13D, and S16D), where overall there was the most overlap with the pure htt-exon1(46Q) oligomers. The peptide-containing oligomers that have less overlap with the pure htt-exon1(46Q) oligomers indicate the peptide has been more efficiently incorporated, and these trends match well with those observed in the ThT aggregation assay. For example, of the three phosphorylation mimicking peptides, T3D displayed the least amount of overlap, and it was the most effective in reducing fibril formation of these three peptides.

With respect to htt, Nt17 domains associate to form the α-helix rich structure of oligomers, bringing polyQ domains into close proximity to promote nucleation.[9, 17, 19, 20, 22, 64] Nt17 peptides inhibit htt fibril formation by incorporating into the α-helix rich oligomer intermediates, increasing the spacing between polyQ domains.[22] This enhanced spacing reduces the efficiency of nucleation. The relative efficiency of the mutant Nt17 peptides to inhibit fibril formation suggests altered ability to incorporate into oligomers. That is, wild type Nt17 peptides readily incorporate into oligomers. Acetylation mimicking mutations reduce the ability to incorporate into oligomers, and Nt17 peptides with phosphorylation mimicking mutations are the least efficiently incorporated into oligomers. Phosphorylation[45, 47, 65] and acetylation[49] within Nt17 of intact htt-exon1 proteins reduce fibril formation, with

phosphorylation having a larger inhibitory effect. This suggests that these post-translational modifications reduce aggregation in full-length htt-exon1 by destabilizing oligomer intermediates and reducing the efficiency of nucleation.

The notion that the effectiveness of Nt17 peptides to impede fibril formation corresponds to their relative incorporation into oligomer intermediates is further supported by altered oligomer morphologies observed by AFM. Reduction of the polyQ and proline-rich domains reduces the protein mass incorporated into oligomers, resulting in small, less rigid oligomers. The largest shift in morphology is observed with free wild-type Nt17, with more efficient incorporation causing a larger reduction in polyQ density that shifts toward smaller oligomers. The peptides mimicking acetylation have an intermediate incorporation and the phosphorylation mimics are least efficiently incorporated; all peptides generally shift to smaller oligomer sizes, but relative to wild-type the shift is less pronounced for acetylation mimics and least pronounced for phosphorylation mimics. Once incorporated, mutations within Nt17 likely impact oligomer stability and the ability of oligomers to undergo nucleation. The incorporation of free Nt17 peptide reduces the polyQ domain density in oligomers, decreasing the local concentration to prevent nucleation and inhibit subsequent fibril formation. With more efficient peptide incorporation, nucleation is more effectively inhibited.

Modifications within Nt17 alters complex formation between peptide and lipids. Nt17 facilitates htt-exon1(46Q) interactions with lipid and can modify aggregation on membranes.[11] Nt17 peptide has a similar interaction mechanism with membranes as htt-exon1(46Q),[32] and the mechanism is not significantly altered by the addition of glutamines.[66] Therefore, synthetic Nt17 peptide with and without modifications was used to

investigate complex formation and determine the degree of membrane interaction between Nt17 and lipids using cVSSI-MS. In this regard, complex refers to combinations of Nt17 derived peptides and specific lipids that are retained after the cVSSI process, suggesting strong association between the peptide and vesicles. To focus on the Nt17 lipid interaction and reduce complications due to varying rates of fibril formation, truncated peptides without the polyQ domain were used for this analysis. Each Nt17 peptide (10 μM) was incubated with POPC/POPS (75/25% w/w) in a 1:10 peptide:lipid molar ratio for 5 h prior to analysis with cVSSI-MS. POPC/POPS was chosen as it promotes a unique htt aggregation pathway that is mediated via Nt17.[42] Experiments were performed in triplicate using positive ion mode. Identified isotopic distributions of each complex were deconvoluted using automated Matlab scripts that determine the individual contributions of each possible configuration of a complex by using theoretical spectra to generate the best fit of the raw data over 1.0×10^6 simulations. The root mean squared deviation (RMSD) between the simulated best fit and the raw data was calculated. For each identified complex, the integrated peak area was calculated by integrating the ion signal for each isotopic distribution of the given complex. Complexes are represented in [M+L] format, where M represents Nt17 peptide and L represents lipid. To correct for plume generation and performance, the integrated peak areas for each complex were normalized to that of the singly-charged POPC lipid monomer ($[L+H]^+$ at *m/z* 760.59), since it was the most abundant peak present across all sample conditions. For final comparisons, integrated peak areas were then represented as a percentage of all peptide-containing ions.

Peptide/lipid complexation was observed to some degree with all peptides studied. Overall, wild-type Nt17 yielded a greater variety of peptide/lipid complexes that were generally

more abundant relative to those of the K6Q, K9Q, and K15Q acetylation mimics and the T3D, S13D, and S16D phosphorylation mimics (Figure 3a). Overall, all peptide complexes followed the same observed trend as wild-type peptide with relative complex abundances of M>2M>3M>4M and increased lipid content further reduced complex abundance such that L>2L>3L. However, the exact lipid contributions for complexes formed by different peptides were more variable. Incubation of wild-type Nt17 peptide with PC/PS lipid yielded eight unique complexes, the most out of all peptides studied, containing upwards of 4M and 3L (Figure 3b, Figure S2a, Table S1). After incubation of the K6Q mutant, three complexes were identified that contained up to 2M and 2L (Figure 3c, Figure S2b, Table S2). The K9Q mutant yielded four complexes after incubation that contained up to 3M and 2L (Figure 3d, Figure S2c, Table S3). Incubation of the K15Q mutant yielded two complexes that contained M and up to 2L (Figure 3e, Figure S2d, Table S4). After the incubation of the T3D mutant, four complexes were identified that contained up to 4M and L (Figure 3f, Figure S2e, Table S5). The S13D mutant yielded five complexes after incubation that contained up to 3M and 2L (Figure 3g, Figure S2f, Table S6). Incubation of the S16D mutant yielded seven complexes that contained up to 4M and 2L (Figure 3h, Figure S2g, Table S7).

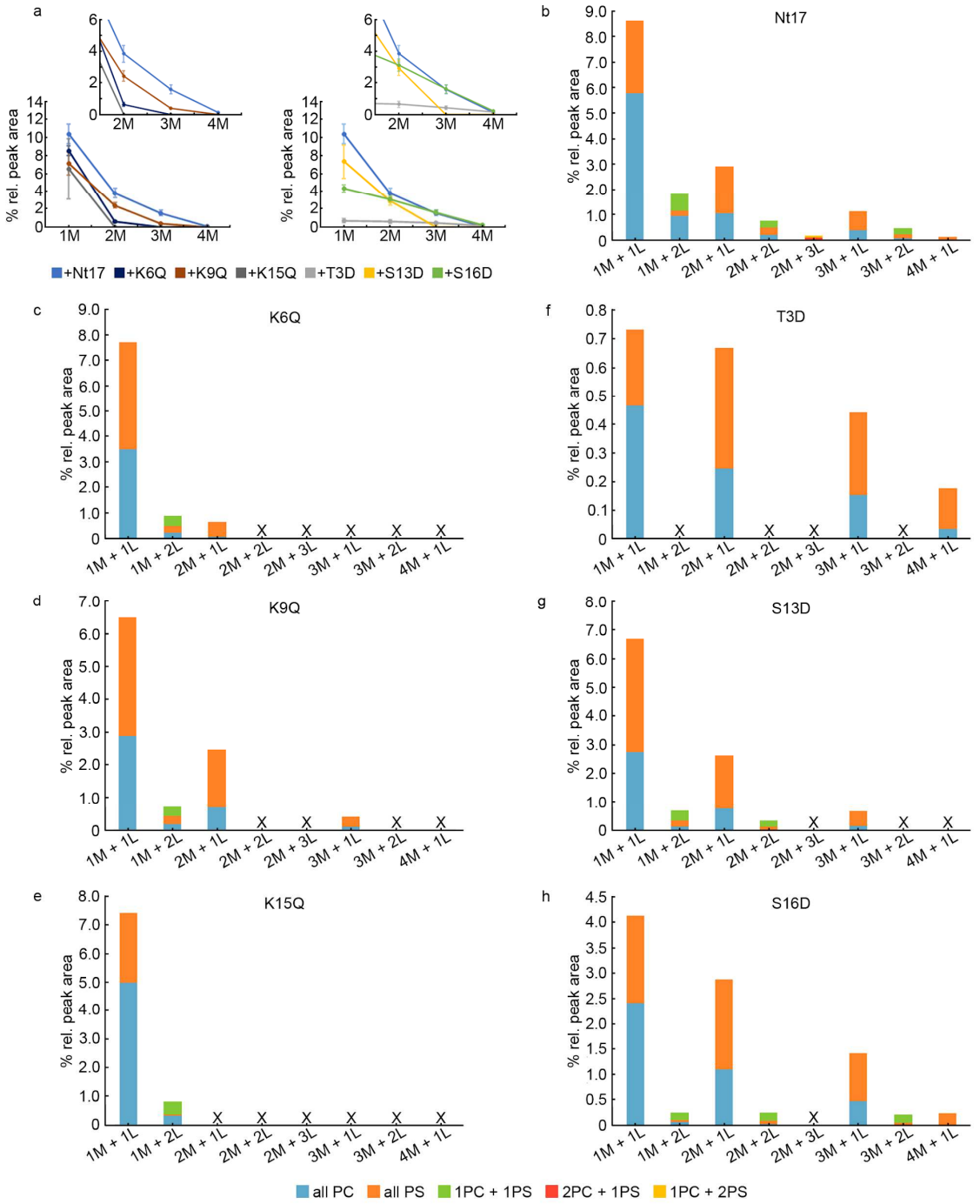

Figure 3: Analysis of Nt17/lipid complexation in the presence of POPC/POPS (75/25% w/w) vesicles using cVSSI-MS. Peptide is denoted as M and lipid as L. The Nt17 peptide concentration was 10 µM and the peptide:lipid ratio was 1:10. (a) The total percent relative peak areas for 1M, 2M, 3M, and 4M complexes identified for each peptide after 5 h incubation with lipid. (b-h) The percent relative peak areas for each identified complex of a given peptide with specified lipid iteration contributions. X indicates that the corresponding complex was not identified for the given condition.

Considering htt demonstrates a preference for anionic lipids[14] and the variation in contribution for different complex configurations, further analysis of complex lipid compositions was performed where the percentage of POPS per complex was evaluated (Figure 4). Analysis revealed that higher order complexes that contain more peptides tend to favor the incorporation of anionic POPS over zwitterionic POPC. For wild-type Nt17, the average POPS composition of the [M+L] complex was 33.05%, [2M+L] was 64.33%, [3M+L] was 67.24%, and [4M+L] was 99.01% (Figure 4a). The average POPS composition for the K6Q mutant complexes [M+L] and [2M+L] were 54.5% and 91.52%, respectively (Figure 4b). For the K9Q mutant, average POPS composition for [M+L] was 55.14%, [2M+L] was 71.77%, and [3M+L] was 80.26% (Figure 4c). The average POPS composition for the K15Q mutant complexes [M+L] and [M+2L] were 29.44% and 19.22%, respectively (Figure 4d). For the T3D mutant the average POPS composition was 36.13% for [M+L], 63.46% for [2M+L], 65.94% for [3M+L], and 81.50% for [4M+L] (Figure 4e). The S13D mutant had average POPS compositions of 57.54% for [M+L], 69.98% for [2M+L], and 75.75% for [3M+L] (Figure 4f). The average POPS composition for the S16D mutant complexes [M+L], [2M+L], [3M+L], and [4M+L] were 41.50%, 61.97%, 67.16%, and 97.48%, respectively (Figure 4g). Despite the clear trend of higher order complexes containing more peptide correlating to increased POPS composition, an increase in the number of lipids incorporated into a complex did not produce a clear trend.

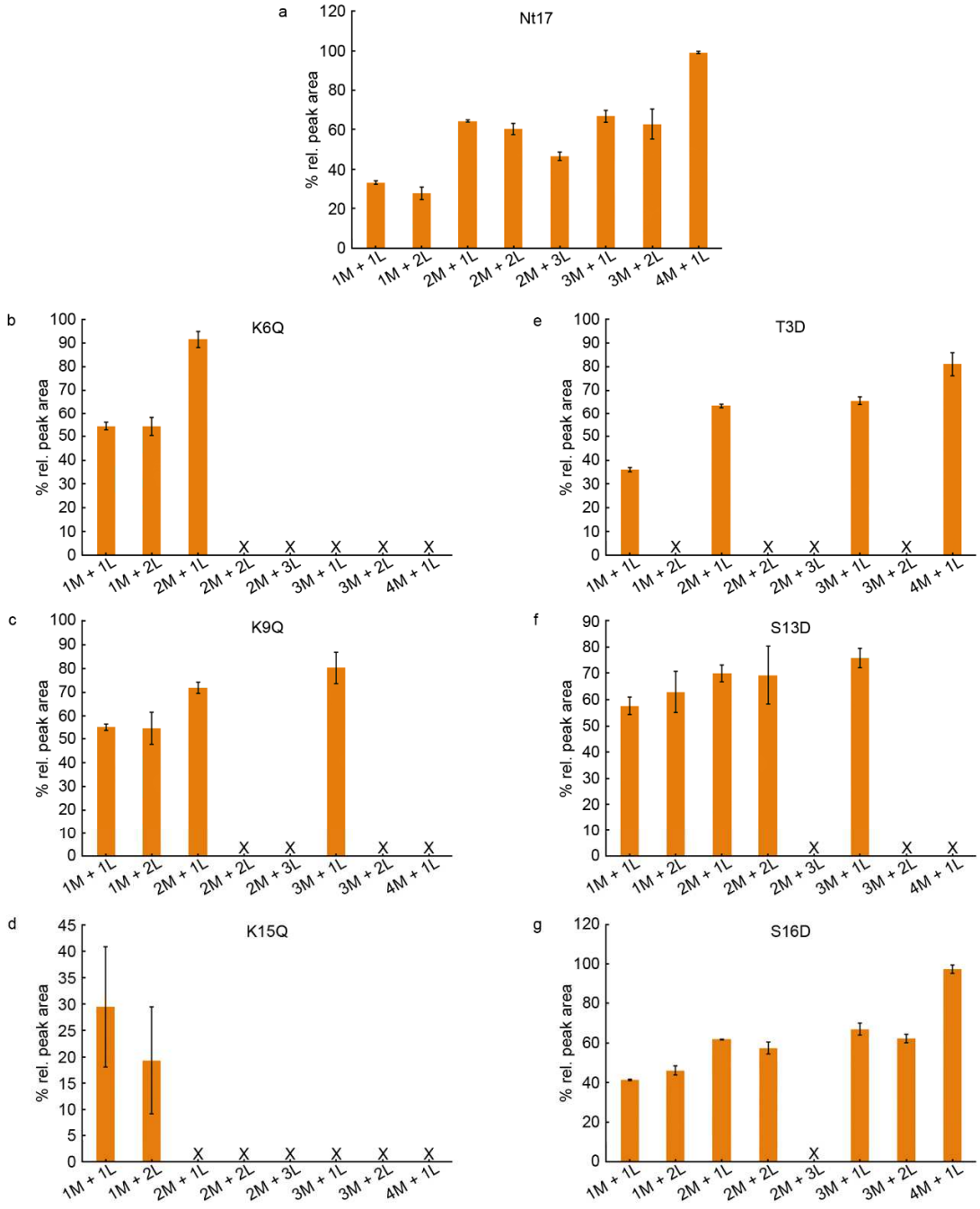

Figure 4: The percent POPS composition for each identified complex of a peptide. X indicates that the corresponding complex was not identified for the given condition. Error bars represent SEM.

For each peptide, the relative peak areas of complexes containing M, 2M, 3M, and 4M peptide were calculated and the percentage of those complexes that contained lipid was determined (Figure 5). For wild-type Nt17, the 4M species only existed as lipid bound (100%), while 3M, 2M, and M complexes were 39.9%, 27.8%, and 12.8% lipid bound, respectively (Figure 5a). For K6Q, only M (8.7%) and 2M (20.7%) complexes contained lipid. 3M complexes were observed, and though none were lipid bound, the 3M complexes were of lower relative peak area than those of the M and 2M (Figure 5b). In the case of K9Q, 8.4% of M, 19.1% of 2M, and 24.6% of 3M complexes were lipid bound (Figure 5c). K15Q only formed M complexes, of which 6.6% were lipid bound (Figure 5d). T3D 4M complexes were always lipid bound (100%) followed by 3M (4.4%), 2M (2.9%), and M (1.1%) complexes (Figure 5e). For S13D, the 2M complexes were more often lipid bound than M complexes, at 16.9% and 9.2% respectively, and much like K6Q, the 3M complexes only existed without lipid but were of lower relative peak area than the M and 2M complexes (Figure 5f). For S16D, M, 2M, 3M, and 4M complexes were observed and 6.6%, 11.8%, 21.4%, and 100% of those complexes, respectively, were lipid bound (Figure 5g). Generally, as peptides formed multimeric species, their probability of being lipid bound increased, suggesting that oligomerization enhances lipid association.

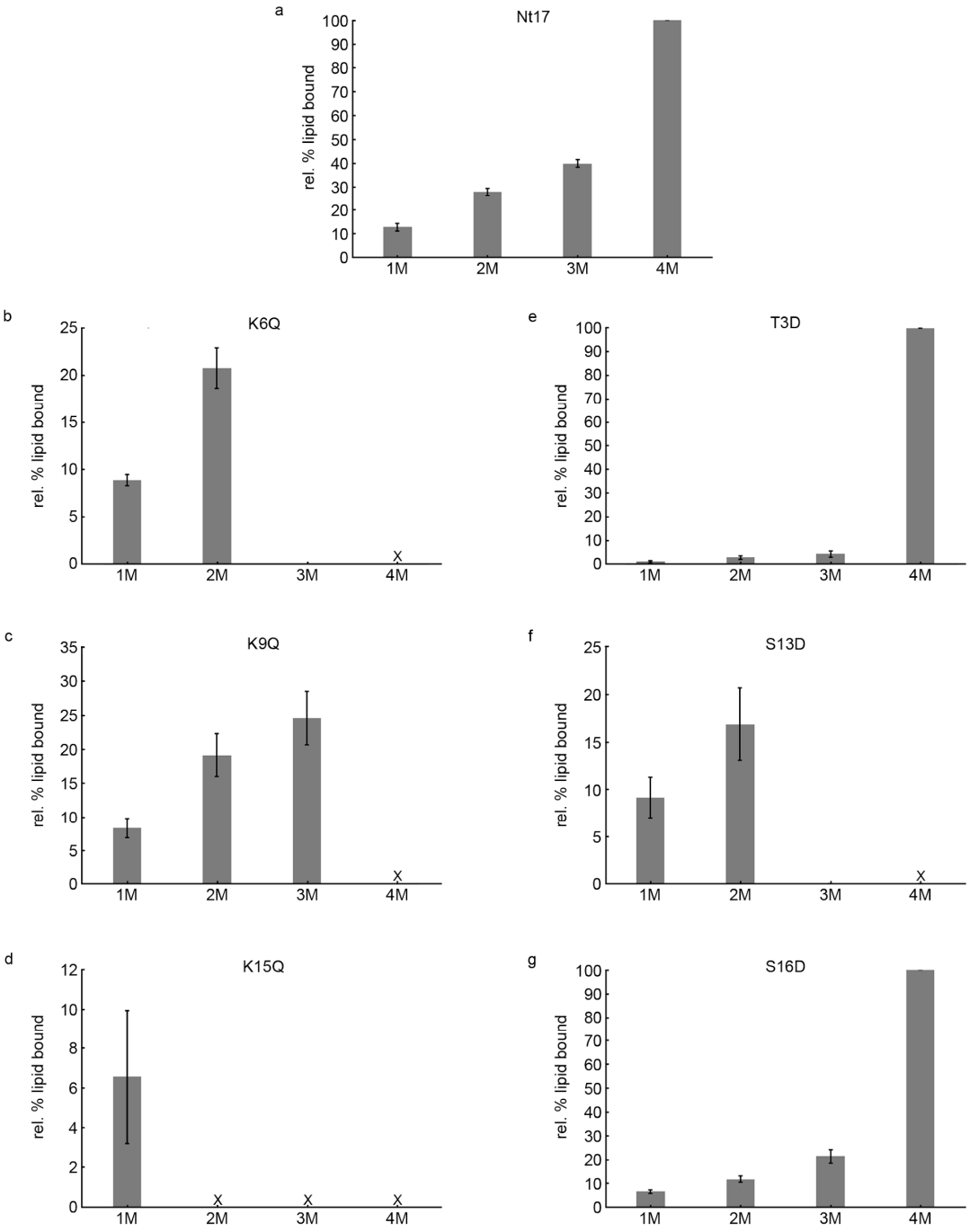

Figure 5: The relative percent of the total monomeric (1M), dimeric (2M), trimeric (3M), and tetrameric (4M) species that are lipid bound for each peptide. Error bars represent SEM. X indicates that species containing that number of peptides were not identified for a given peptide. If no X is indicated and no bar is present, all species identified for that number of peptides did not contain lipid.

Nt17 facilitates lipid interactions via a transition to an amphipathic α-helix,[13, 23] a transition that still occurs even with mutations mimicking acetylation and phosphorylation. Previous studies have demonstrated that acetylation does not alter α-helical structure with respect to lipid binding,[49] and the phosphomimic mutations also do not alter secondary peptide structure.[46, 48] The interaction between Nt17 and lipid bilayers is summed up in four general steps: approach, reorganization, anchoring, and insertion.[66] Generally the approach step is driven by charged residues within Nt17; when Nt17 is exposed to a POPE membrane, early interactions occur between the membrane and S13, K15, or S16.[66] Once at the membrane surface, the structure and orientation of Nt17 is stabilized by salt bridges formed between the membrane and peptide residues K6, K9, and E12 and by hydrogen bonding between the membrane and peptide involving residues T3 and S13.[66] Another important consideration is the role of lipid composition in Nt17/lipid interactions, as changes to lipid composition can impact Nt17 approach and overall orientation at the membrane surface[41] in addition to the degree of insertion.[67] For pure POPC membranes, Nt17 favors a C-terminal approach where S13, K15, and S16 are close to the membrane surface, while T3, K6, and K9 broadly sample orientations ranging from parallel to antiparallel with the membrane surface.[41] POPC/POPS vesicles demonstrate stronger interactions with Nt17 compared to pure POPC vesicles, and increasing POPS content increases Nt17 affinity for the membrane, demonstrating a major electrostatic contribution to peptide/membrane interactions where F11 inserts into the membrane to anchor the peptide.[67] With these considerations, it is likely that the mutations in this study alter the approach of the peptide and stabilizing interactions at the membrane surface, including electrostatics, salt-bridge formation, and hydrogen bonding.

Oligomer/lipid interactions are modified by the incorporation of modified Nt17 peptides.

Considering the ThT assays and AFM experiments indicate that oligomerization and subsequent nucleation is altered in addition to Nt17/lipid complexation, and with oligomeric species being the most lipid active,[68] further characterization of oligomeric interactions with respect to lipid binding was necessary. To determine the impact incorporating free Nt17 peptides into oligomeric structures had on their ability to bind lipids, a colorimetric/fluorescent membrane binding assay with lipid/PDA vesicles was used. The lipid systems utilized in these experiments were TBLE and POPC/POPS (75/25% w/w). The additional TBLE system was used to provide a more physiologically relevant mixture of lipid components. TBLE was not used in the cVSSI-MS analysis presented previously because of the complexity of this model system is not amenable to straightforward analysis. When exposed to proteins, the fluorescence of each system directly correlates to the extent of protein/lipid interaction, and the fluorescent signals for all conditions were normalized to the htt-exon1(46Q) control and averaged across all runs (Figure 6). For all experiments, htt-exon1(46Q) oligomers with and without the incorporation of Nt17 peptides were generated by 3 h of incubation, providing starting oligomers consistent with those analyzed by AFM in Figure 2.

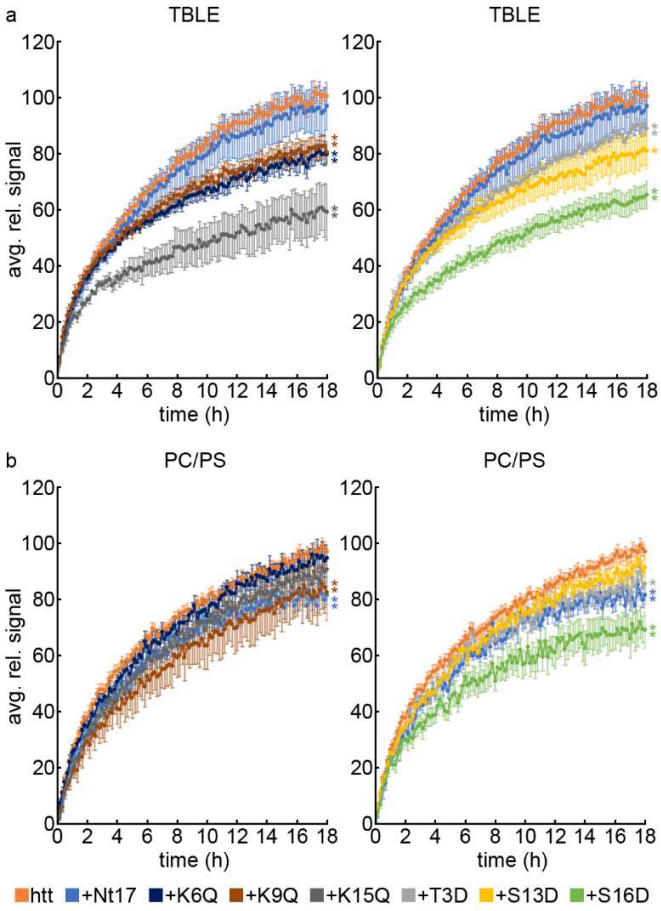

Figure 6: PDA/lipid binding assays for htt-exon1(46Q) incubated alone or with each Nt17 peptide in the presence of (a) TBLE or (b) PC/PS. Htt-exon1(46Q) concentration was 10 µM, and the protein:peptide ratio was 1:1. All conditions were calculated and averaged across all runs then normalized as a percentage to the htt-exon1(46Q) control. Error bars represent SEM. Using a Student's t-test, * represents a p-value of <0.05 and ** represents a p-value of <0.01 relative to the htt-exon1(46Q) control.

The incubation of htt-exon1(46Q) oligomers with free Nt17 peptides generally reduced interactions with TBLE relative to oligomers composed purely of htt-exon1(46Q) (Figure 6a). Oligomers containing free, wild-type Nt17 peptides demonstrated virtually no change in lipid interactions. However, oligomers containing peptides mimicking acetylation showed significant reductions in lipid binding ($p<0.01$ for all three peptides). Specifically, the K15Q mutant had the greatest impact, with approximately a 40% reduction in signal relative to the htt-exon1(46Q)

control. The K6Q and K9Q mutants each demonstrated approximately a 20% reduction in signal relative to the htt-exon1(46Q) control. Oligomers containing peptides mimicking phosphorylation also showed significant reductions in lipid binding ($p<0.01$ for T3D and S16D, $p<0.05$ for S13D). Oligomers containing S16D mutant peptides had the largest impact, with approximately a 35% reduction in signal. Though less significant statistically, oligomers containing S13D peptides demonstrated approximately a 20% reduction in signal. Oligomers containing T3D peptides had the lowest impact, with an approximately 10% reduction in signal.

In the case of the PC/PS lipid system, generally the impacts of incorporating free Nt17 peptides were less than those observed with TBLE (Figure 6b). Oligomers containing free, wild-type Nt17 peptides showed a significant reduction in signal ($p<0.01$) of approximately 15%. For oligomers containing peptides mimicking acetylation, only the K9Q peptide showed a significant reduction in signal ($p<0.01$) by approximately 15%. The K6Q and K15Q peptide-containing oligomers showed no significant changes in lipid interactions relative to the htt-exon1(46Q) control. For oligomers containing peptides mimicking phosphorylation, only those containing S16D and T3D peptides showed significant reductions in lipid binding ($p<0.01$ and $p<0.05$ respectively). Oligomers containing S16D peptides showed approximately a 30% reduction in signal, while those containing T3D peptides had less of an impact with approximately a 10% reduction in signal relative to the htt-exon1(46Q) control.

It has been demonstrated that certain residues are crucial to stabilizing multimeric structures once Nt17 transitions to an α-helical structure. Specifically, the potential electrostatic interaction between K15 and E11 can help stabilize the dimer-dimer interface in a tetrameric structure.[13] The removal of positive charges by carbethoxylation favors monomeric

conformations of Nt17, as monomeric conformations become more abundant with increasing modification while multimeric species are destabilized and decrease in abundance as detected by IMS-MS.[18] Molecular dynamics studies indicated that K6 is likely involved in the stabilization of dimeric species through interactions with E12 and S16,[18] while K9 is implicated in intramolecular salt bridges with E5 and/or E12. [14, 49] With both S13 and S16 being solvent exposed, modification to these residues could be involved in the packing of tetrameric structures into higher order species necessary for oligomer stabilization to facilitate fibril formation.[45] Oligomer stability as a function of introducing mutations mimicking acetylation and phosphorylation could be another dominant factor in altered oligomer/lipid interactions as shown in PDA assays. Generally, there appears to be larger consequences for changes made to the C-terminus, as modification of K15 had the largest impact among the acetylation mimics while the S16 mutant had the largest impact among phosphorylation mutants.

CONCLUSIONS

The process of amyloid formation and subsequent interactions is very complex and can be modulated by a variety of factors including PTMs [45-50, 53, 54, 68, 69] and the overall cellular environment.[70-72] In this study, the impacts of free Nt17 peptides with mutations mimicking acetylation (removal of a positive charge) and phosphorylation (addition of a negative charge) on htt aggregation, aggregate morphologies, protein/lipid complexation, and lipid interactions were evaluated. With regard to a htt-exon1(46Q) protein, the addition of all free Nt17 peptides significantly reduced fibril formation, with wild-type Nt17 being the most effective and completely inhibiting fibril formation, followed by acetylation mimics then

phosphorylation mimics. The incorporation of free Nt17 peptides into oligomeric structures resulted in a shift in aggregate morphology, with wild-type Nt17 causing the largest deviation in morphology from pure htt-exon1(46Q) oligomers, followed by acetylation mimics then phosphorylation mimics. The ability of the different peptides to complex with lipids was also altered, with wild-type Nt17 forming the most unique peptide/lipid complexes that were generally more abundant than those identified for the acetylation and phosphorylation mimics. However, despite changes to the degree of peptide/lipid complexation across the peptides studied, they all showed preferential interaction with anionic POPS lipid over zwitterionic POPC lipid for higher order complexes that contained more peptide. Generally, higher order complexes were also more frequently lipid bound overall. When free peptides were incorporated into oligomers that were then exposed to lipid vesicles, the degree of interaction between the oligomers and different lipid systems was dependent on the free peptide incorporated in addition to the lipid composition. The data suggests complicated interactions beginning at the monomeric level that translate to altered interactions at the oligomeric level, and that such interactions are influenced by factors such as local peptide charge and the environment.

ACKNOWLEDGEMENTS

We acknowledge the use of the WVU Shared Research Facilities and funding from the National Institutes of Health (R01GM135432). ARS was supported by a Ruby Distinguished Doctoral Fellowship from WVU.

REFERENCES

[1] Huntington's Disease Collaborative Research Group, A novel gene containing a trinucleotide repeat that is exanded and unstable on Huntingtons-disease chromosomes Cell, 72 (1993) 971-983.
[2] R.G. Snell, J.C. Macmillan, J.P. Cheadle, I. Fenton, L.P. Lazarou, P. Davies, M.E. Macdonald, J.F. Gusella, P.S. Harper, D.J. Shaw, Relationship between trinucleotide repeat expansion and phenotypic variation in Huntingtons-disease, Nat. Genet., 4 (1993) 393-397.
[3] J.B. Penney, J.P. Vonsattel, M.E. MacDonald, J.F. Gusella, R.H. Myers, CAG repeat number governs the development rate of pathology in Huntington's disease, Ann. Neurol., 41 (1997) 689-692.
[4] E. Scherzinger, R. Lurz, M. Turmaine, L. Mangiarini, B. Hollenbach, R. Hasenbank, G.P. Bates, S.W. Davies, H. Lehrach, E.E. Wanker, Huntingtin-encoded polyglutamine expansions form amyloid-like protein aggregates in vitro and in vivo, Cell, 90 (1997) 549-558.
[5] E. Scherzinger, A. Sittler, K. Schweiger, V. Heiser, R. Lurz, R. Hasenbank, G.P. Bates, H. Lehrach, E.E. Wanker, Self-assembly of polyglutamine-containing huntingtin fragments into amyloid-like fibrils: Implications for Huntington's disease pathology, P. Nat. Acad. Sci. USA, 96 (1999) 4604-4609.
[6] S.M. Chen, V. Berthelier, J.B. Hamilton, B. O'Nuallain, R. Wetzel, Amyloid-like features of polyglutamine aggregates and their assembly kinetics, Biochemistry, 41 (2002) 7391-7399.
[7] A. Adegbuyiro, F. Sedighi, A.W. Pilkington, S. Groover, J. Legleiter, Proteins Containing Expanded Polyglutamine Tracts and Neurodegenerative Disease, Biochemistry, 56 (2017) 1199-1217.
[8] J.R. Arndt, M. Chaibva, J. Legleiter, The emerging role of the first 17 amino acids of huntingtin in Huntington's disease, BioMolecular Concepts, 6 (2015) 33-46.
[9] A.K. Thakur, M. Jayaraman, R. Mishra, M. Thakur, V.M. Chellgren, I.-J.L. Byeon, D.H. Anjum, R. Kodali, T.P. Creamer, J.F. Conway, A.M. Gronenborn, R. Wetzel, Polyglutamine disruption of the huntingtin exon 1 N terminus triggers a complex aggregation mechanism, Nat. Struct. Mol. Biol., 16 (2009) 380-389.
[10] G. Darnell, J.P.R.O. Orgel, R. Pahl, S.C. Meredith, Flanking polyproline sequences inhibit beta-sheet structure in polyglutamine segments by inducing PPII-like helix structure, J. Mol. Biol., 374 (2007) 688-704.
[11] K.A. Burke, K.J. Kauffman, C.S. Umbaugh, S.L. Frey, J. Legleiter, The Interaction of Polyglutamine Peptides with Lipid Membranes Is Regulated by Flanking Sequences Associated with Huntingtin, J. Biol. Chem., 288 (2013) 14993-15005.
[12] A. Nagarajan, S. Jawahery, S. Matysiak, The Effects of Flanking Sequences in the Interaction of Polyglutamine Peptides with a Membrane Bilayer, J. Phys. Chem. B, 118 (2014) 6368-6379.
[13] M. Michalek, E.S. Salnikov, B. Bechinger, Structure and Topology of the Huntingtin 1-17 Membrane Anchor by a Combined Solution and Solid-State NMR Approach, Biophys. J., 105 (2013) 699-710.
[14] S. Cote, V. Binette, E.S. Salnikov, B. Bechinger, N. Mousseau, Probing the Huntingtin 1-17 Membrane Anchor on a Phospholipid Bilayer by Using All-Atom Simulations, Biophys. J., 108 (2015) 1187-1198.

[15] X.L. Wang, A. Vitalis, M.A. Wyczalkowski, R.V. Pappu, Characterizing the conformational ensemble of monomeric polyglutamine, Proteins, 63 (2006) 297-311.
[16] A. Vitalis, X. Wang, R.V. Pappu, Quantitative characterization of intrinsic disorder in polyglutamine: Insights from analysis based on polymer theories, Biophys. J., 93 (2007) 1923-1937.
[17] S.A. Kotler, V. Tugarinov, T. Schmidt, A. Ceccon, D.S. Libich, R. Ghirlando, C.D. Schwieters, G.M. Clore, Probing initial transient oligomerization events facilitating Huntingtin fibril nucleation at atomic resolution by relaxation-based NMR, P. Nat. Acad. Sci. USA, 116 (2019) 3562-3571.
[18] J.R. Arndt, S.G. Kondalaji, M.M. Maurer, A. Parker, J. Legleiter, S.J. Valentine, Huntingtin N-Terminal Monomeric and Multimeric Structures Destabilized by Covalent Modification of Heteroatomic Residues, Biochemistry, 54 (2015) 4285-4296.
[19] V.N. Sivanandam, M. Jayaraman, C.L. Hoop, R. Kodali, R. Wetzel, P.C.A. van der Wel, The Aggregation-Enhancing Huntingtin N-Terminus Is Helical in Amyloid Fibrils, J. Am. Chem. Soc., 133 (2011) 4558-4566.
[20] M. Jayaraman, R. Kodali, B. Sahoo, A.K. Thakur, A. Mayasundari, R. Mishra, C.B. Peterson, R. Wetzel, Slow Amyloid Nucleation via alpha-Helix-Rich Oligomeric Intermediates in Short Polyglutamine-Containing Huntingtin Fragments, J. Mol. Biol., 415 (2012) 881-899.
[21] M. Jayaraman, R. Mishra, R. Kodali, A.K. Thakur, L.M.I. Koharudin, A.M. Gronenborn, R. Wetzel, Kinetically Competing Huntingtin Aggregation Pathways Control Amyloid Polymorphism and Properties, Biochemistry, 51 (2012) 2706-2716.
[22] R. Mishra, M. Jayaraman, B.P. Roland, E. Landrum, T. Fullam, R. Kodali, A.K. Thakur, I. Arduini, R. Wetzel, Inhibiting the Nucleation of Amyloid Structure in a Huntingtin Fragment by Targeting alpha-Helix-Rich Oligomeric Intermediates, J. Mol. Biol., 415 (2012) 900-917.
[23] M. Michalek, E.S. Salnikov, S. Werten, B. Bechinger, Membrane Interactions of the Amphipathic Amino Terminus of Huntingtin, Biochemistry, 52 (2013) 847-858.
[24] S.H. Li, X.J. Li, Huntingtin-protein interactions and the pathogenesis of Huntington's disease, Trends Genet., 20 (2004) 146-154.
[25] E. Cattaneo, C. Zuccato, M. Tartari, Normal huntingtin function: an alternative approach to Huntington's disease, Nat. Rev. Neurosci., 6 (2005) 919-930.
[26] K.E. De Rooij, J.C. Dorsman, M.A. Smoor, J.T. Den Dunnen, G.J. Van Ommen, Subcellular localization of the Huntington's disease gene product in cell lines by immunofluorescence and biochemical subcellular fractionation, Hum. Mol. Genet., 5 (1996) 1093-1099.
[27] J. Xia, D.H. Lee, J. Taylor, M. Vandelft, R. Truant, Huntingtin contains a highly conserved nuclear export signal, Hum. Mol. Genet., 12 (2003) 1393-1403.
[28] R.S. Atwal, J. Xia, D. Pinchev, J. Taylor, R.M. Epand, R. Truant, Huntingtin has a membrane association signal that can modulate huntingtin aggregation, nuclear entry and toxicity, Hum. Mol. Genet., 16 (2007) 2600-2615.
[29] M. Gu, M.T. Gash, V.M. Mann, F. Javoy-Agid, J.M. Cooper, A.H. Schapira, Mitochondrial defect in Huntington's disease caudate nucleus, Ann. Neurol., 39 (1996) 385-389.
[30] A.V. Panov, C.-A. Gutekunst, B.R. Leavitt, M.R. Hayden, J.R. Burke, W.J. Strittmatter, J.T. Greenamyre, Early mitochondrial calcium defects in Huntington's disease are a direct effect of polyglutamines, Nat. Neuro., 5 (2002) 731-736.

[31] Y.S. Choo, G.V.W. Johnson, M. MacDonald, P.J. Detloff, M. Lesort, Mutant huntingtin directly increases susceptibility of mitochondria to the calcium-induced permeability transition and cytochrome c release, Hum. Mol. Genet., 13 (2004) 1407-1420.
[32] D.T.W. Chang, G.L. Rintoul, S. Pandipati, I.J. Reynolds, Mutant huntingtin aggregates impair mitochondrial movement and trafficking in cortical neurons, Neurobiol. Dis., 22 (2006) 388-400.
[33] A.L. Orr, S. Li, C.-E. Wang, H. Li, J. Wang, J. Rong, X. Xu, P.G. Mastroberardino, J.T. Greenamyre, X.-J. Li, N-terminal mutant huntingtin associates with mitochondria and impairs mitochondrial trafficking, J. Neurosci., 28 (2008) 2783-2792.
[34] K.-Y. Liu, Y.-C. Shyu, B.A. Barbaro, Y.-T. Lin, Y. Chern, L.M. Thompson, C.-K.J. Shen, J.L. Marsh, Disruption of the nuclear membrane by perinuclear inclusions of mutant huntingtin causes cell-cycle re-entry and striatal cell death in mouse and cell models of Huntington's disease, Hum. Mol. Genet., 24 (2015) 1602-1616.
[35] K.B. Kegel, E. Sapp, J. Yoder, B. Cuiffo, L. Sobin, Y.J. Kim, Z.H. Qin, M.R. Hayden, N. Aronin, D.L. Scott, F. Isenberg, W.H. Goldmann, M. DiFiglia, Huntingtin associates with acidic phospholipids at the plasma membrane, J. Biol. Chem., 280 (2005) 36464-36473.
[36] F.J.B. Bäuerlein, I. Saha, A. Mishra, M. Kalemanov, A. Martinez-Sanchez, R. Klein, I. Dudanova, M.S. Hipp, F.U. Hartl, W. Baumeister, R. Fernandez-Busnadiego, In Situ Architecture and Cellular Interactions of PolyQ Inclusions, Cell, 171 (2017) 179-+.
[37] N. Riguet, A.L. Mahul-Mellier, N. Maharjan, J. Burtscher, M. Croisier, G. Knott, J. Hastings, A. Patin, V. Reiterer, H. Farhan, S. Nasarov, H.A. Lashuel, Nuclear and cytoplasmic huntingtin inclusions exhibit distinct biochemical composition, interactome and ultrastructural properties, Nat. Commun., 12 (2021) 6579.
[38] F. Gasset-Rosa, C. Chillon-Marinas, A. Goginashvili, R.S. Atwal, J.W. Artates, R. Tabet, V.C. Wheeler, A.G. Bang, D.W. Cleveland, C. Lagier-Tourenne, Polyglutamine-Expanded Huntingtin Exacerbates Age-Related Disruption of Nuclear Integrity and Nucleocytoplasmic Transport, Neuron, 94 (2017) 48-57.e44.
[39] M. Beasley, A.R. Stonebraker, I. Hasan, K.L. Kapp, B.J. Liang, G. Agarwal, S. Groover, F. Sedighi, J. Legleiter, Lipid Membranes Influence the Ability of Small Molecules To Inhibit Huntingtin Fibrillization, Biochemistry, 58 (2019) 4361-4373.
[40] G.R. Levy, K. Shen, Y. Gavrilov, P.E.S. Smith, Y. Levy, R. Chan, J. Frydman, L. Frydman, Huntingtin's N-Terminus Rearrangements in the Presence of Membranes: A Joint Spectroscopic and Computational Perspective, ACS Chem. Neuro., 10 (2019) 472-481.
[41] M. Beasley, N. Frazee, S. Groover, S.J. Valentine, B. Mertz, J. Legleiter, Physicochemical Properties Altered by the Tail Group of Lipid Membranes Influence Huntingtin Aggregation and Lipid Binding, J. Phys. Chem. B, 126 (2022) 3067-3081.
[42] N.K. Pandey, J.M. Isas, A. Rawat, R.V. Lee, J. Langen, P. Pandey, R. Langen, The 17-residue-long N terminus in huntingtin controls stepwise aggregation in solution and on membranes via different mechanisms, J. Biol. Chem., 293 (2018) 2597-2605.
[43] M. Beasley, S. Groover, S.J. Valentine, J. Legleiter, Lipid headgroups alter huntingtin aggregation on membranes, BBA - Biomembranes, 1863 (2021) 183497.
[44] M. Chaibva, X. Gao, P. Jain, W.A. Campbell, S.L. Frey, J. Legleiter, Sphingomyelin and GM1 Influence Huntingtin Binding to, Disruption of, and Aggregation on Lipid Membranes, ACS Omega, 3 (2018) 273-285.

[45] R. Mishra, C.L. Hoop, R. Kodali, B. Sahoo, P.C.A. van der Wel, R. Wetzel, Serine Phosphorylation Suppresses Huntingtin Amyloid Accumulation by Altering Protein Aggregation Properties, J. Mol. Biol., 424 (2012) 1-14.
[46] A. Chiki, S.M. DeGuire, F.S. Ruggeri, D. Sanfelice, A. Ansaloni, Z.M. Wang, U. Cendrowska, R. Burai, S. Vieweg, A. Pastore, G. Dietler, H.A. Lashuel, Mutant Exon1 Huntingtin Aggregation is Regulated by T3 Phosphorylation-Induced Structural Changes and Crosstalk between T3 Phosphorylation and Acetylation at K6, Angew. Chem., 56 (2017) 5202-5207.
[47] C.T. Aiken, J.S. Steffan, C.M. Guerrero, H. Khashwji, T. Lukacsovich, D. Simmons, J.M. Purcell, K. Menhaji, Y.-Z. Zhu, K. Green, F. LaFerla, L. Huang, L.M. Thompson, J.L. Marsh, Phosphorylation of Threonine 3: Implications for Huntingtin aggregation and Neurotoxicity, J. Biol. Chem., 284 (2009) 29427-29436.
[48] S.M. DeGuire, F.S. Ruggeri, M.B. Fares, A. Chiki, U. Cendrowska, G. Dietler, H.A. Lashuel, N-terminal Huntingtin (Htt) phosphorylation is a molecular switch regulating Htt aggregation, helical conformation, internalization, and nuclear targeting, J. Biol. Chem., 293 (2018) 18540-18558.
[49] M. Chaibva, S. Jawahery, A.W. Pilkington, J.R. Arndt, O. Sarver, S. Valentine, S. Matysiak, J. Legleiter, Acetylation within the First 17 Residues of Huntingtin Exon 1 Alters Aggregation and Lipid Binding, Biophys. J., 111 (2016) 349-362.
[50] M.A. Kalchman, R.K. Graham, G. Xia, H.B. Koide, J.G. Hodgson, K.C. Graham, Y.P. Goldberg, R.D. Gietz, C.M. Pickart, M.R. Hayden, Huntingtin is ubiquitinated and interacts with a specific ubiquitin-conjugating enzyme, J. Biol. Chem., 271 (1996) 19385-19394.
[51] M. Stefani, C.M. Dobson, Protein aggregation and aggregate toxicity: new insights into protein folding, misfolding diseases and biological evolution, J. Mol. Med., 81 (2003) 678-699.
[52] F. Sedighi, A. Adegbuyiro, J. Legleiter, SUMOylation Prevents Huntingtin Fibrillization and Localization onto Lipid Membranes, ACS Chem. Neuro., 11 (2020) 328-343.
[53] S.E. Groover, M. Beasley, V. Ramamurthy, J. Legleiter, Phosphomimetic Mutations Impact Huntingtin Aggregation in the Presence of a Variety of Lipid Systems, Biochemistry, 59 (2020) 4681-4693.
[54] Y. Wang, F. Lin, Z.H. Qin, The role of post-translational modifications of huntingtin in the pathogenesis of Huntington's disease, Neurosci. Bull., 26 (2010) 153-162.
[55] G. Burra, A.K. Thakur, Inhibition of polyglutamine aggregation by SIMILAR huntingtin N-terminal sequences: Prospective molecules for preclinical evaluation in Huntington's disease, Biopolymers, 108 (2017).
[56] B. Hollenbach, E. Scherzinger, K. Schweiger, R. Lurz, H. Lehrach, E.E. Wanker, Aggregation of truncated GST-HD exon 1 fusion proteins containing normal range and expanded glutamine repeats, Philos. Trans. R. Soc. Lond. B Bio.l Sci., 354 (1999) 991-994.
[57] P.J. Muchowski, G. Schaffar, A. Sittler, E.E. Wanker, M.K. Hayer-Hartl, F.U. Hartl, Hsp70 and Hsp40 chaperones can inhibit self-assembly of polyglutamine proteins into amyloid-like fibrils, P. Nat. Acad. Sci. USA, 97 (2000) 7841-7846.
[58] F. Zheng, Z. Wu, Y. Chen, A quantitative method for the measurement of membrane affinity by polydiacetylene-based colorimetric assay, Anal. Biochem., 420 (2012) 171-176.
[59] T. Kowalewski, J. Legleiter, Imaging stability and average tip-sample force in tapping mode atomic force microscopy, J. Appl. Phys., 99 (2006).

[60] J. Legleiter, R.B. DeMattos, D.M. Holtzman, T. Kowalewski, In situ AFM studies of astrocyte-secreted apolipoprotein E- and J-containing lipoproteins, J. Colloid Interface. Sci., 278 (2004) 96-106.
[61] K.A. Burke, J. Godbey, J. Legleiter, Assessing mutant huntingtin fragment and polyglutamine aggregation by atomic force microscopy, Methods, 53 (2011) 275-284.
[62] C. Li, K. Attanayake, S.J. Valentine, P. Li, Facile Improvement of Negative Ion Mode Electrospray Ionization Using Capillary Vibrating Sharp-Edge Spray Ionization, Anal. Chem., 92 (2020) 2492-2502.
[63] N. Ranganathan, C. Li, T. Suder, A.K. Karanji, X. Li, Z. He, S.J. Valentine, P. Li, Capillary Vibrating Sharp-Edge Spray Ionization (cVSSI) for Voltage-Free Liquid Chromatography-Mass Spectrometry, J. Am. Soc.Mass Spec., 30 (2019) 824-831.
[64] T.E. Williamson, A. Vitalis, S.L. Crick, R.V. Pappu, Modulation of Polyglutamine Conformations and Dimer Formation by the N-Terminus of Huntingtin, J. Mol. Biol., 396 (2010) 1295-1309.
[65] X. Gu, E.R. Greiner, R. Mishra, R. Kodali, A. Osmand, S. Finkbeiner, J.S. Steffan, L.M. Thompson, R. Wetzel, X.W. Yang, Serines 13 and 16 Are Critical Determinants of Full-Length Human Mutant Huntingtin Induced Disease Pathogenesis in HD Mice, Neuron, 64 (2009) 828-840.
[66] S. Cote, G. Wei, N. Mousseau, Atomistic mechanisms of huntingtin N-terminal fragment insertion on a phospholipid bilayer revealed by molecular dynamics simulations, Proteins, 82 (2014) 1409-1427.
[67] M. Michalek, C. Aisenbrey, B. Bechinger, Investigation of membrane penetration depth and interactions of the amino-terminal domain of huntingtin: refined analysis by tryptophan fluorescence measurement, Eur. Biophys. J., 43 (2014) 347-360.
[68] F. Sedighi, A. Skeens, A. Adegbuyiro, J. Bard, C. Siriwardhana, E. Donley, W.J. Geldenhuys, J. Legleiter, Oligomerization enhances huntingtin membrane activity but is suppressed by covalent crosslinking, bioRxiv, (2023) 2023.2003.2001.530665.
[69] J.S. Steffan, N. Agrawal, J. Pallos, E. Rockabrand, L.C. Trotman, N. Slepko, K. Illes, T. Lukacsovich, Y.Z. Zhu, E. Cattaneo, P.P. Pandolfi, L.M. Thompson, J.L. Marsh, SUMO modification of Huntingtin and Huntington's disease pathology, Science, 304 (2004) 100-104.
[70] K.A. Burke, E.A. Yates, J. Legleiter, Biophysical insights into how surfaces, including lipid membranes, modulate protein aggregation related to neurodegeneration, Fron. Neurol., 4 (2013).
[71] G.P. Gorbenko, P.K.J. Kinnunen, The role of lipid-protein interactions in amyloid-type protein fibril formation, Chem. Phys. Lipids, 141 (2006) 72-82.
[72] C. Aisenbrey, T. Borowik, R. Byström, M. Bokvist, F. Lindström, H. Misiak, M.A. Sani, G. Gröbner, How is protein aggregation in amyloidogenic diseases modulated by biological membranes?, Eur. Biophys. J., 37 (2008) 247-255.

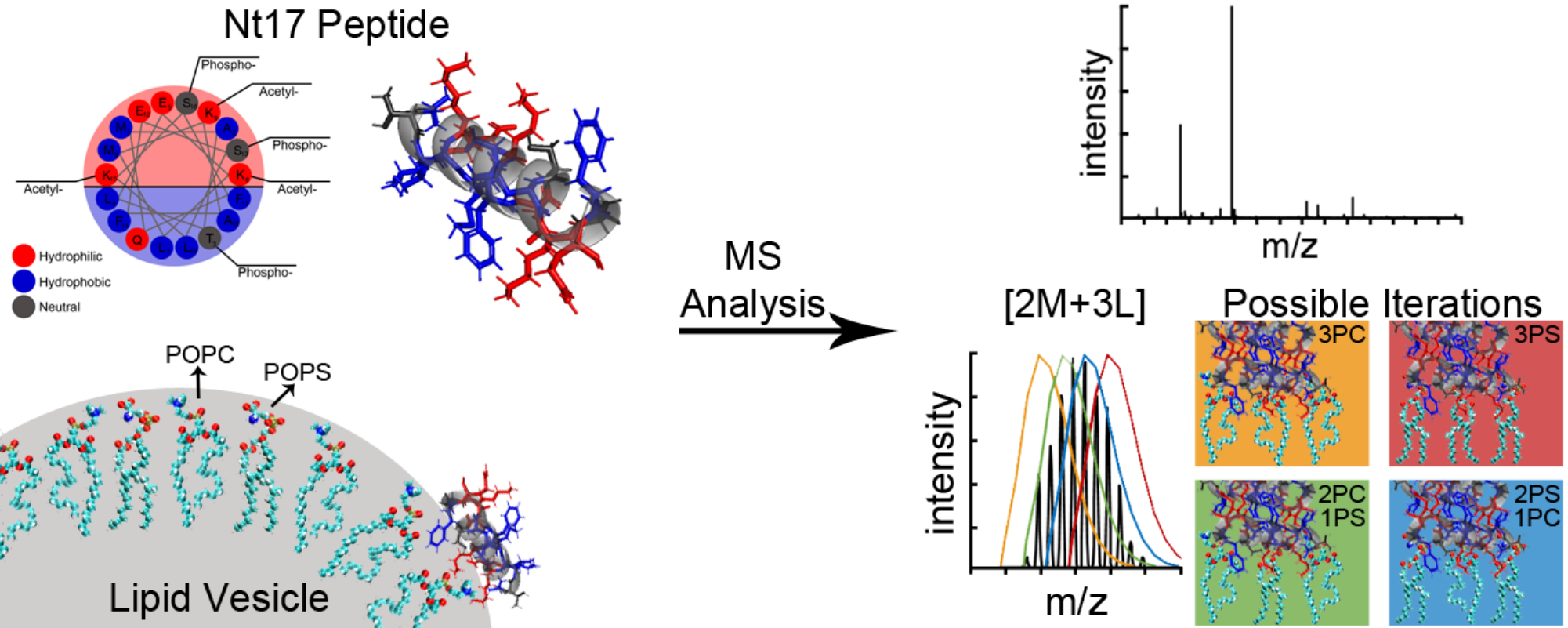
Nt17 Peptide
Phospho-
Acetyl-
Phospho-
Acetyl-
Acetyl-
Phospho-
Hydrophilic
Hydrophobic
Neutral
POPC
POPS
Lipid Vesicle
MS
Analysis
intensity
m/z
[2M+3L]
intensity
m/z
Possible Iterations
3PC
3PS
2PC
1PS
2PS
1PC